Electronic Supplementary Material (ESI) for Journal of Materials Chemistry A.

Biohybrid architectures for efficient light-to-current conversion based on photosystem I within scalable 3D mesoporous electrodes

K. R. Stieger*[a], S. C. Feifel[a], H. Lokstein[b], M. Hejazi[c], A. Zouni[c] and F. Lisdat*[a]

A) Calculation of the electro-active surface of a µITO structure

The electroactive surface of µITO structure was calculated as follows: First cyclic voltammetry measurements of a defined surface area (geometrical surface: 0.2 cm^2) of flat ITO (pre-cleaned by ultrasonication in acetone, isopropanol and water) and of 2, 4, 6, 8 x µITO (geometrical surface: 0.2 cm^2) have been performed from -300 – +400 mV vs. Ag/AgCl at RT in phosphate buffer (5 mM, pH 7) without any redox species. At 0 mV vs. Ag/AgCl (dI/dV = 0) the charging currents (anodic and cathodic) have been determined and averaged (n = 4). Here, we assume that the electroactive surface of flat ITO is corresponding to its geometrical surface and that the electrochemical double layer structure is similar for ITO and µITO. This means higher charging currents are only caused by a higher surface area in contact with the electrolyte. Consequently, the electroactive surface area is calculated for the µITO out of the charging current increase of µITO compared to flat ITO.

I) Cyclic voltammetry of 6x µITO, 6x µITO-cyt *c*, 6x µITO-PSI-cyt *c* and µITO-PSI electrodes

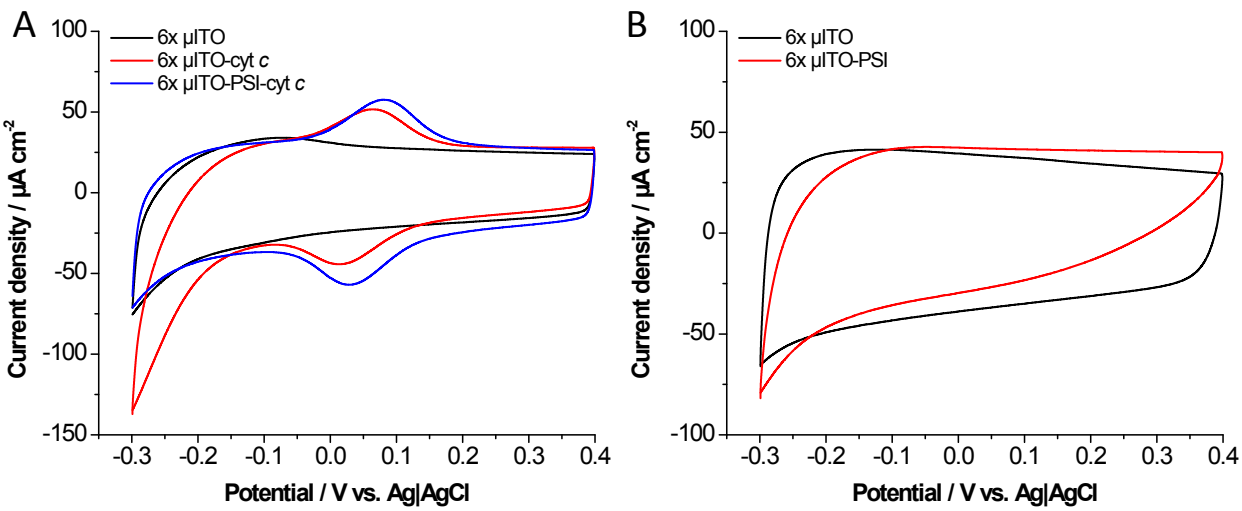

Figure S1. Cyclic voltammograms of different 6x µITO electrodes: **A)** CV of a bare 6xµITO, a 6x µITO-cyt *c* and a 6x µITO-PSI-cyt *c* electrode. **(B)** CV of a bare 6xµITO and a 6xµITO/PSI electrode. No redox signals can be detected when only PSI is immobilized in the structure. The experiments have been performed in the dark at a scan rate of 10 mV s^{-1} in aerobic phosphate buffer (5 mM, pH 7).

II) Photocatalysis of 6x µITO-PSI-cyt *c* electrodes

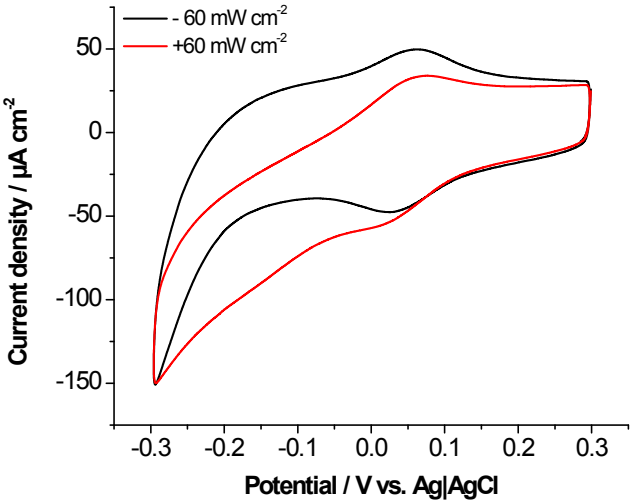

Figure S2. Photo-induced catalytic current of the 6x µITO-PSI-cyt *c* electrode. The experiment has been performed in the dark (black) and with 60 mW cm^{-2} of white light (red) at a scan rate of 10 mV s^{-1} in aerobic phosphate buffer (5 mM, pH 7) as well as 1 mM methyl viologen. In the dark only the redox conversion of cyt *c* can be seen at around 45 mV vs. Ag/AgCl. Cathodic catalysis under illumination starts at a potential at which cyt *c* can be reduced by the electrode. This means that first electrons are transfered from the µITO to cyt *c* before PSI reduction by cyt *c* occurs.

III) Photocurrent control: µITO-PSI, µITO-cyt *c*, µITO

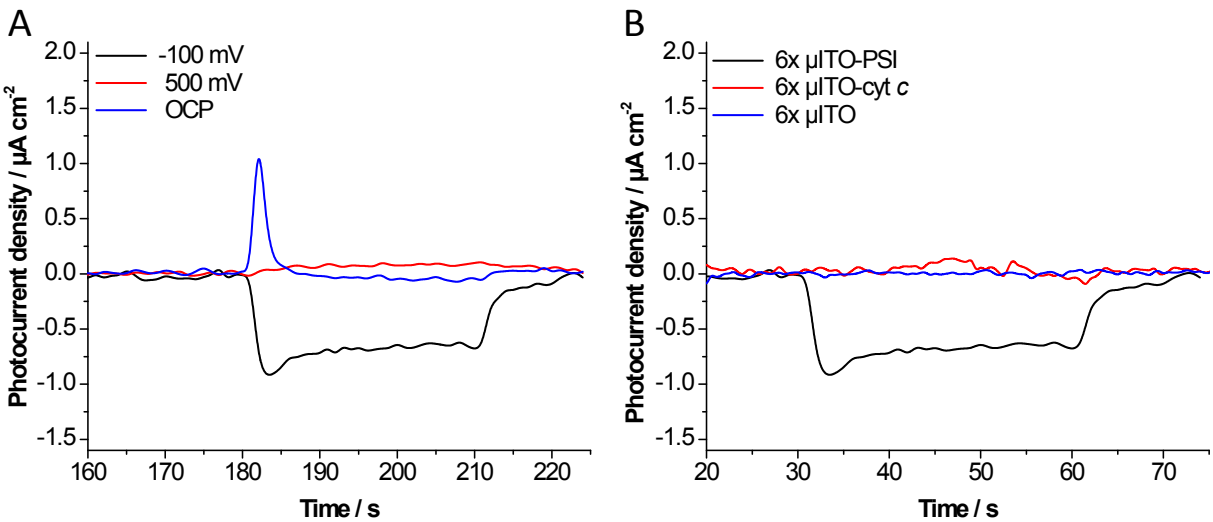

Figure S3. Photocurrent measurements of the 6x µITO-PSI, 6x µITO-cyt *c* and 6x µITO electrodes. **(A)** The photocurrent measurements at three different potentials of a 6x µITO-PSI (-100 mV, +500 mV, OCP = 196 mV vs. Ag/AgCl) exhibit only minor photocurrent densities, cathodic but no anodic photocurrents are observed (left). This experiment shows, that cyt *c* is necessary for the high unidirectional photocurrent generation. The direct electron transfer from PSI to the µITO electrode is highly limited. **(B)** Comparison of photocurrents achieved at a potential of -100 mV vs. Ag/AgCl between 6x µITO-PSI, 6x µITO-cyt *c* and 6x µITO electrodes. Without PSI in the structure there is no photocurrent detected. All experiments have been performed at RT in phosphate buffer (5 mM, pH 7) using white light (20 mW cm^{-2}, 30 s pulse).

IV) Photocurrent of 6x µITO-PSI-cyt *c* electrodes in buffer of higher ionic strength

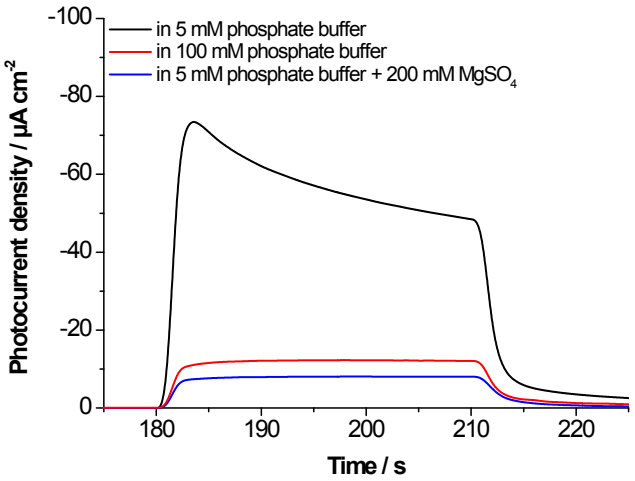

Figure S4. Photocurrent measurements of the 6x µITO-PSI-cyt *c* electrode. Due to higher concentration of either buffer substance (100 mM phosphate) or addition of 200 mM $MgSO_4$, photocurrents decrease significantly. The experiments have been performed at RT in phosphate buffer (5 mM, pH 7) using white light (20 mW cm^{-2}, 30 s pulse) at a potential of -100 vs. Ag/AgCl.

V) Surface area of air-sintered/air plasma-treated µITO electrodes

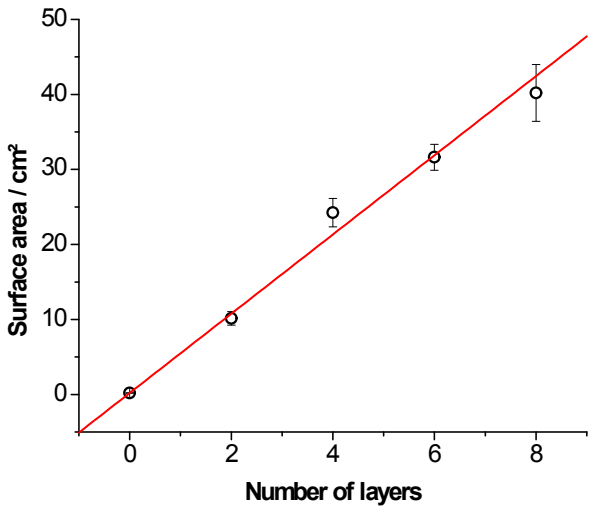

Figure S5. Surface area increase dependent on the number of applied layers for an air sintered µITO electrode. The surface increases by 5.3 ± 0.2 cm^2 / layer (R^2 = 0.995, n = 4).

VI) Determination of the heterogeneous electron transfer rate constant (k_s) for a µITO-cyt *c* electrode

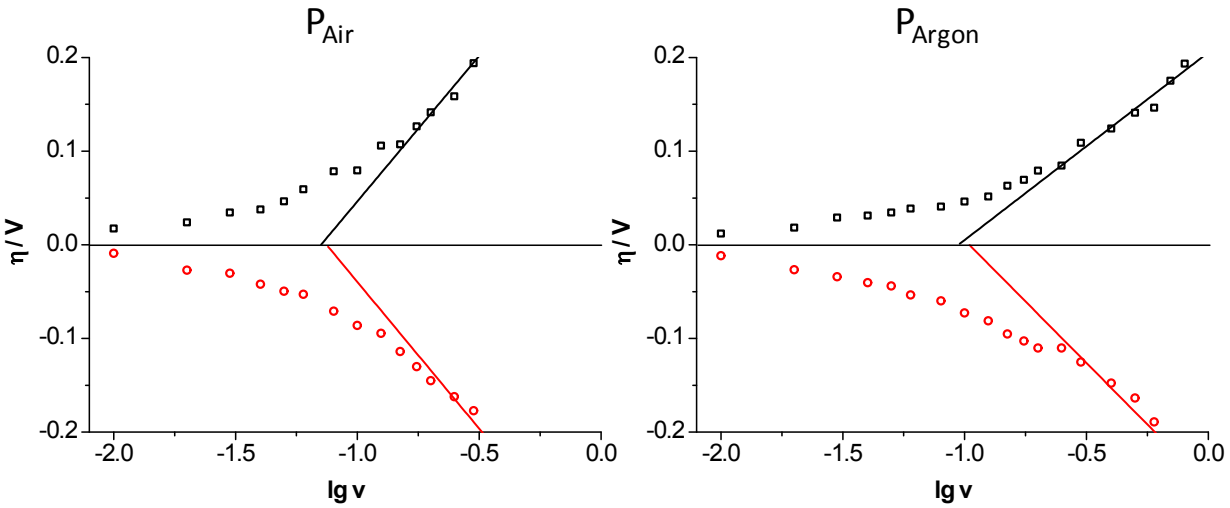

Figure S6. Trumpet plot for the determination of k_s after the method of Laviron for P_{Air} (left) and P_{Argon} (right). The overpotential ($E_0 - E_p$) for both anodic (black) and cathodic (red) peaks is plotted against the decadic logarithm of the scan rate (lg v). A linear fit of the data with a peak separation of > 200 mV results in a slope proportional to the charge transfer coefficient (α) with an intercept proportional to k_s.

VII) Transmission spectra of ITO and 6x µITO structures

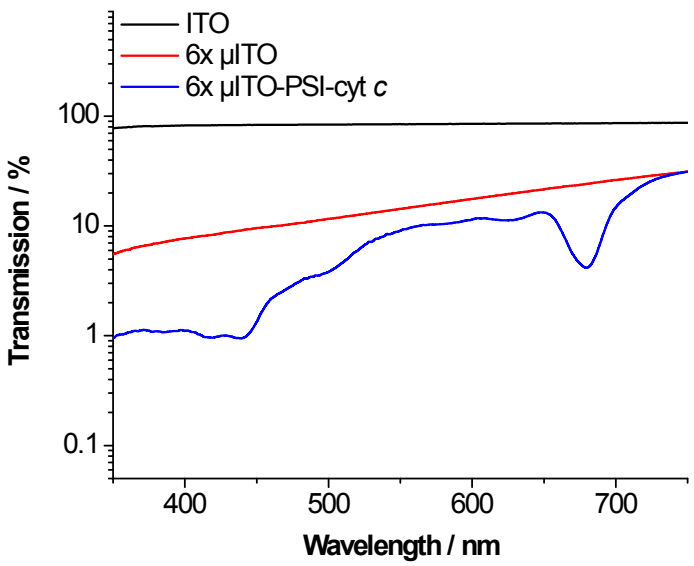

Figure S7. Transmission spectrum of ITO, 6x µITO and 6x µITO-PSI-cyt *c* electrodes.

VII) Spectrum of the white light source

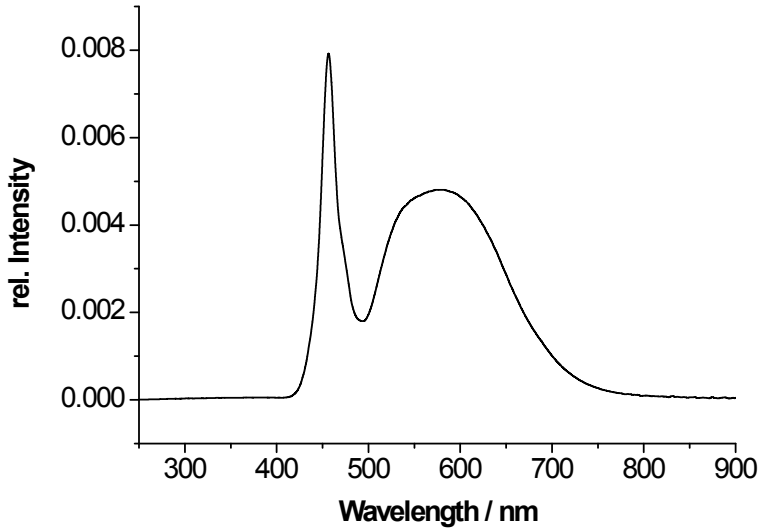

Figure S8. Spectrum of the white light source used in all experiments. The spectrum was normalized to an integral area of 1. Characteristic peaks are found at 456 nm and 576 nm.